crystals

MDPI

Article

Synthesis, Crystal Structure, DFT Theoretical Calculationand Physico-Chemical Characterization of a New Complex Material $(C_6H_8Cl_2N_2)_2[Cd_3Cl_{10}]\cdot 6H_2O$

Sabrine Hermi [1], Mohammed G. Althobaiti [2], Abdullah A. Alotaibi [3], Abdulhadi H. Almarri [4], Wataru Fujita [5], Frédéric Lefebvre [6], Cherif Ben Nasr [1] and Mohamed Habib Mrad [1,3,*]

1 Laboratoire de Chimie des Matériaux, Faculté des Science de Bizerte, Université de Carthage, Jarzounz 7021, Tunisia; sabrin94hermi@gmail.com (S.H.); cherif_bennasr@yahoo.fr (C.B.N.)
2 Department of Physics, College of Science, Taif University, P.O. Box 11099, Taif 21944, Saudi Arabia; M.althobaiti@tu.edu.sa
3 Department of Chemistry, College of Sciences and Humanities, Shaqra University, Ad-Dawadmi 11911, Saudi Arabia; aaalotaibi@su.edu.sa
4 Department of Chemistry, College-Allwajh University of Tabuk, Tabuk 71421, Saudi Arabia; aalmarri@ut.edu.sa
5 General Education, Faculty of Science and Technology, Seikei University, Kichijoji-Kitamachi, Musashino 180-8633, Japan; fujitaw@st.seikei.ac.jp
6 Laboratoire de ChimieOrganométallique de Surface (LCOMS), Ecole Supérieure de Chimie Physique Electronique, CEDEX, 69626 Villeurbanne, France; fg_lefebvre@hotmail.fr
* Correspondence: m.mrad@su.edu.sa

Abstract: The chemical preparation, crystal structure, Hirshfeld surface analysis and spectroscopic characterization of the novel cadmium (II) 2,5-dichloro-*p*-phenylendiaminium decachlorotricadmate(II) hexahydrate complex, $(C_6H_8Cl_2N_2)_2[Cd_3Cl_{10}]\cdot 6H_2O$, has been reported. The atomic arrangement can be described as built up by an anionic framework, formed by edge-sharing $[CdCl_6]^{2-}$ octahedra in linear polymeric chains spreading along the *a*-axis, while the organic cations surround these latters. The inspection of the Hirshfeld surface analysis helps to discuss the strength of hydrogen bonds and to quantify the inter-contacts, which reveal that H ... Cl/Cl ... H (38.9%), H ... H (13.9%), and Cd ... Cl/Cl ... Cd (12.4%) are the main interactions that govern the crystal packing of the studied structure. SEM/EDXwas carried out and the powder XRD confirmed the good crystallinity of the material. FT-IR and the DFT calculation reveal the good correlation between the experimental and the theoretical wavenumbers. The HOMO-LUMO energy gap was used to predict the electric conductivity of the compound. Finally, the thermal TGA/DTA analysis shows stability until 380 K.

Keywords: cadmium hybrid material; X-ray diffraction; DFT; Hirshfeld surface; enrichment ratio; SEM/EDX; IR absorption; thermal analysis

check for updates

Citation: Hermi, S.; Althobaiti, M.G.; Alotaibi, A.A.; Almarri, A.H.; Fujita, W.; Lefebvre, F.; Ben Nasr, C.; Mrad, M.H. Synthesis, Crystal Structure, DFT Theoretical Calculationand Physico-Chemical Characterization of a New Complex Material $(C_6H_8Cl_2N_2)_2[Cd_3Cl_{10}]\cdot 6H_2O$. *Crystals* **2021**, *11*, 553. https://doi.org/10.3390/cryst11050553

Academic Editor: Paola Paoli

Received: 15 April 2021
Accepted: 11 May 2021
Published: 15 May 2021

Publisher's Note: MDPI stays neutral with regard to jurisdictional claims in published maps and institutional affiliations.

Copyright: © 2021 by the authors. Licensee MDPI, Basel, Switzerland. This article is an open access article distributed under the terms and conditions of the Creative Commons Attribution (CC BY) license (https://creativecommons.org/licenses/by/4.0/).

1. Introduction

In recent years, great efforts have been developed for hybrid materials. In fact, the idea behind these types of materials is to optimize both organic and inorganic components on the molecular scale and the expected material takes advantage of organic (such as polymerizable and mesomorphism) and inorganic moieties (such as conductivity), where their properties are strongly dependent on their structures [1–7].

The approach is based on the identification of the hydrogen bond acceptor sites, as their sites with the hydrogen bond donors have the potential to afford organized crystalline arrays in different dimensions [8–10]. In fact, amines are commonly selected as potential hydrogen bonding donors and metal halides are particularly considered as strong hydrogen bond acceptors. Particularly, 2,5-dichloro-*p*-phenylendiamine is an organic molecule which contains two amino groups on the aromatic ring. It is a good template

presenting both rigidity and flexibility and is also rarely studied. The non-planarity and the stabilization of the amine is the result of a balance between two opposing forces: the conjugation of the nitrogen lone pair with the aromatic ring [11]. This latter is a very useful in several fields such as microelectronics and electromagnetic sensors, due to the high environmental stability, and controllable electrical conductivity [12–14]. However, it should be emphasized that solid-state structures arise from a balance of intermolecular forces. Although stronger forces may dominate, weaker forces (donor-acceptor interactions, and dispersion forces) are also important and may lead together to the development of the three-dimensional network [9].The association of protonated organic cations and metallic-based moieties, either anions or polyatomic clusters, led to a remarkable diversity of assemblies. As metal halides, halocadmates(II) have received considerable attention thanks to their polymorphic behavior, electronic configuration, and lattice location. Moreover, their structural diversity is the key issue in semiconductor physics, supramolecular studies, and bioinorganic studies [15–18].

The principal goal of this work is to give detailed information about the anionic polymeric part of the considered compound with respect to its physicochemical properties. Thus, in order to examine the interactions inside the supramolecular arrangement, it is important to study their quantitative measurements.

2. Experimental

2.1. Elaboration of $(C_6H_8Cl_2N_2)_2[Cd_3Cl_{10}]\cdot 6H_2O$

The studied compound $(C_6H_8Cl_2N_2)_2[Cd_3Cl_{10}]\cdot 6H_2O$ was prepared by an acid-base reaction between HCl, cadmium chloride and 2,5-dichloro-p-phenylenediaminein in a stoichiometric amount 3:2.

A 5.5 g of $CdCl_2$ (3×10^{-2} mol) was mixed with HCl (purity 37%) and neutralized by 2×10^{-2} mol of 2,5-dichloro-p-phenylenediamine (3.5 g, purity 97%) dissolved in ethanol.

After three weeks, colorless plate crystals adequate for XRD study were obtained with dimensions of $0.4 \times 0.15 \times 0.15$ mm^3.

The chemical reaction scheme is:

$$3CdCl_2 + 2C_6H_8Cl_2N_2 + 4HCl + 4H_2O \rightarrow (C_6H_8Cl_2N_2)_2[Cd_3Cl_{10}]\cdot 6H_2O$$

The elemental analysis technique is used in order to determine the proposed formula: C (12.43%/12.45%); H (2.41%/2.44%); N (4.83%/4.84%) (exp/theor).

2.2. Charactrisation

2.2.1. X-ray Powder Diffraction (XRPD) Analysis

PXRD pattern was recorded using a Siemens D 5000 diffractometer (λ = 1.542 Å) with 2θ in the range 5–50°.

2.2.2. X-ray Single-Crystal Structural Analysis

The X-ray diffraction data were collected at 150 K using a Rigaku AFC system equipped with graphitmonochromatedMoKα radiation. The absorption corrections were made with the help of the Rigaku/MSC Crystal clear package [19]. The structure was solved by a dual space method with the Olex 2 program and refined by successive differential Fourier syntheses and performed on F^2 by a full matrix least squares procedure using the Olex2.refine program [20,21].

The structure of $(C_6H_8Cl_2N_2)_2[Cd_3Cl_{10}]\cdot 6H_2O$ was developed in the centrosymmetric space group $P\bar{1}$. The drawings were made with Diamond2.0 [22] and the structural graphics of the asymmetric unit were created with Mercury 3.8 [23].

2.2.3. Morphologies and EDX Analysis

SEM micrographs were observed on JEOL-6610LV electron microscope at an acceleration voltage of 20 kV, with a magnification of 500× and 1500×, coupled with Oxford X-Max microanalysis system EDX.

2.2.4. Spectroscopic Measurements

The (FT-IR) spectrum was registeredusing a NICOLET IR 200 between 4000 and 500 cm^{-1}.

2.2.5. Thermal Study

The TGA/DTA was performed with a PYRIS 1TG machine on 12.772 mg with a scanning rate of 5 $Kmin^{-1}$ under a dynamic argon atmosphere from 300 to 1100 K.

2.2.6. DFT Calculation

Theoretical calculations were made on the two organic ligands and on the Cd_3Cl_{13} group as defined in the asymmetric unit. All calculationswere made using the DFT/B3LYP/LanL2DZ basis set for all atoms. The software used is Gaussian A-09, except for the boundary orbital calculations for which Gaussian-98was used. The results were analyzed with Molekel (border orbitals and MEP), Gauss-Sum (IR and orbital distribution (DOS)) and Molden (preparation of files, analysis of optimizations and spectra) softwares.

3. Results and Discussion

3.1. SEM Morphologies and EDX Analysis

SEM/EDX is a technique that has been used to observe the size, morphology and to determine the elemental composition of the crystal. Figure 1a shows the surface morphology of $(C_6H_8Cl_2N_2)_2[Cd_3Cl_{10}]\cdot 6H_2O$. As it can be seen, the surface is uniformly made by an assembly of fine particles with a stick form.

Additionally, in order to verify the elements present in the studied material, the EDX profile has been recorded and is shown in Figure 1b. The spectrum confirms the presence of Cd, Cl, N, C, and O in the target material.

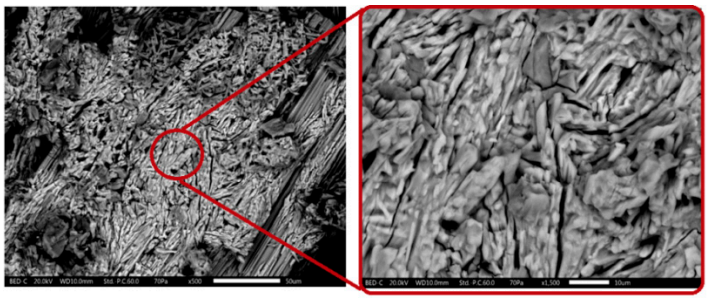

(**a**)

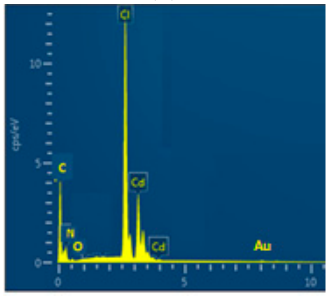

(**b**)

Figure 1. SEM images of $(C_6H_8Cl_2N_2)_2[Cd_3Cl_{10}]\cdot 6H_2O$ for a magnification 500 times (left) and 1500 times (right) (**a**). EDX spectrum in the zone of high contrast (**b**).

3.2. X-ray Powder Diffraction (XRPD) Analysis

Figure 2 compares the XRPD pattern of the compound $(C_6H_8Cl_2N_2)_2[Cd_3Cl_{10}]\cdot 6H_2O$ with those generated from the single-crystal data. The overlaid simulated XRDP closely resembles the experimental pattern at the majority of the positions of the peaks.

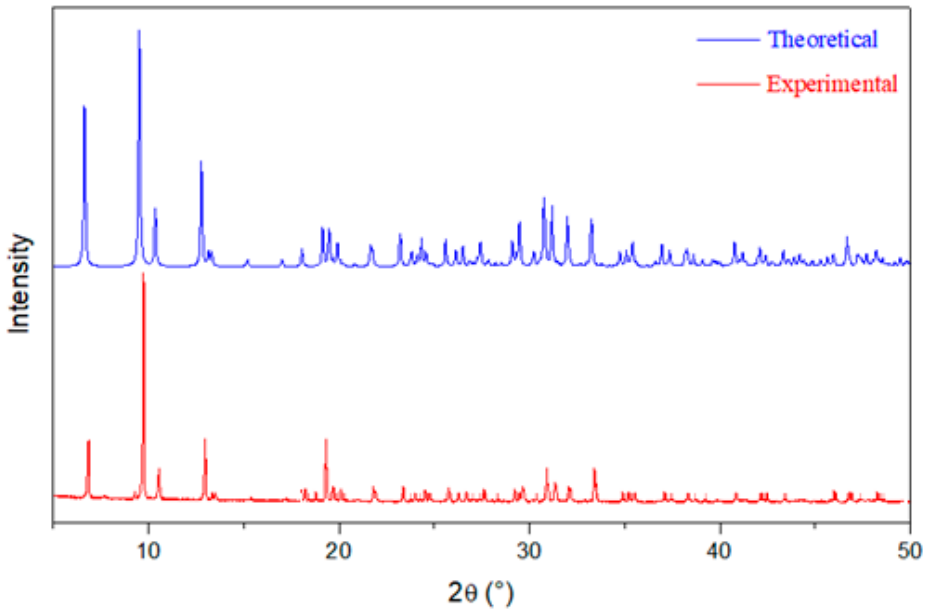

Figure 2. Theoretical and experimental XRPD of $(C_6H_8Cl_2N_2)_2[Cd_3Cl_{10}]\cdot 6H_2O$.

3.3. Crystal Structure Description

The asymmetric unit consists of two halves of $(C_6H_8Cl_2N_2)^{2+}$, three water molecules and one half of $[Cd_3Cl_{10}]^{4-}$ anion, formed by cadmium atom Cd(1) located on an inversion center at (0,0,1/2) and Cd(2)(Figure 3). It is worth noting that the water molecules O10 are disordered equally over two positions with a molar ratio of 0.5:0.5 (O10A and O10B). The crystal data and the experimental parameters used for the intensity data collection are reported in Table 1. Selected bonds and angles are listed in Table 2; Table 3.

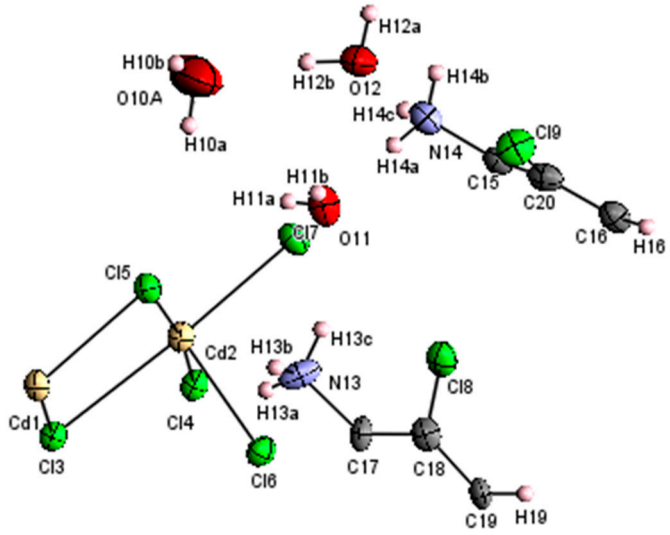

Figure 3. ORTEP representation of $(C_6H_8Cl_2N_2)_2[Cd_3Cl_{10}]\cdot 6H_2O$.

Table 1. Crystallographic Details.

Crystal Data	
Chemical formula	$Cd_3Cl_{10}·2(C_6H_8Cl_2N_2)·6(H_2O)$
M_r	1157.95
Crystal system, space group	Triclinic, $P\bar{1}$
Temperature (K)	150
a, b, c (Å)	6.784 (4), 9.552 (6), 13.592 (9)
α, β, γ (°)	102.247 (9), 92.665 (11), 97.160 (7)
V (Å^3)	851.6 (9)
Z	1
Radiation type	Mo $K\alpha$
μ (mm^{-1})	2.99
Crystal size (mm)	0.4 × 0.15 × 0.15
Data Collection	
Diffractometer	Rigaku Mercury
Absorption correction:	Multi-scan
T_{min}, T_{max}	0.421, 0.638
No. of measured, independent and observed [$F^2 > 2.0\sigma(F^2)$] reflections	9842, 3887, 3357
R_{int}	0.071
$(\sin\theta/\lambda)_{max}$ (Å^{-1})	0.650
Refinement	
$R[F^2 > 2\sigma(F^2)]$, $wR(F^2)$, S	0.041, 0.100, 1.11
No. of reflections	3887
No. of parameters	198
No. of restraints	5
$\Delta\rho_{max}$, $\Delta\rho_{min}$ (e Å^{-3})	0.99, −1.57
CCDC No	2061865

The crystal packing is formed by a polymeric chains of $[Cd_3Cl_{10}]_n^{4n-}$ anions propagating parallel to the *a*-axis (Figure 4). These chains, located at z = $\frac{1}{2}$, are made by edge-sharing $CdCl_6$ octahedra, where the $[C_6H_8Cl_2N_2]^{2+}$ and H_2O are inserted between these chains.

The stability and cohesion of the atomic arrangement are made via a large number of hydrogen bonds between the cations and the inorganic polymeric chains: N14–H13C ... Cl6, N13–H13B ... Cl5, N13–H13A ... Cl6 and N13–H13B ... O11 hydrogen bonds (Table 4).

For the inorganic entity, two types of cadmium chloride octahedral are observed: $Cd(1)Cl_6$ and $Cd(2)Cl_6$, which give rise to a polymeric chain of $[Cd_3Cl_{10}]_n^{4n-}$ along the *b*-axis. Figure 5 shows that the $Cd(1)Cl_6$ octahedron shares one bridging chlorine atoms (Cl(4) and Cl(3)) with the $Cd(2)Cl_6$ ocathedra, generated by a symmetric center, share one bridging chlorine atoms (Cl(3) and Cl(3′)). Moreover, the bond length and angles vary with the environment around the Cl atoms. The value of the Cd-Cl bond lengths are in the range 2.527–2.818 Å. The average bridging Cd-Cl distances, of 2.6695 Å, are longer than the terminal ones, equal to 2.5936 Å, and the Cl-Cd-Cl bond angles vary from 168.21 to 180° [24–28]. These distortionsare most likely caused by the interaction of the NH_3^+ groups with the chloride pairs that affect the distortion of the $CdCl_6$ units via Cd^{2+} lone pair.

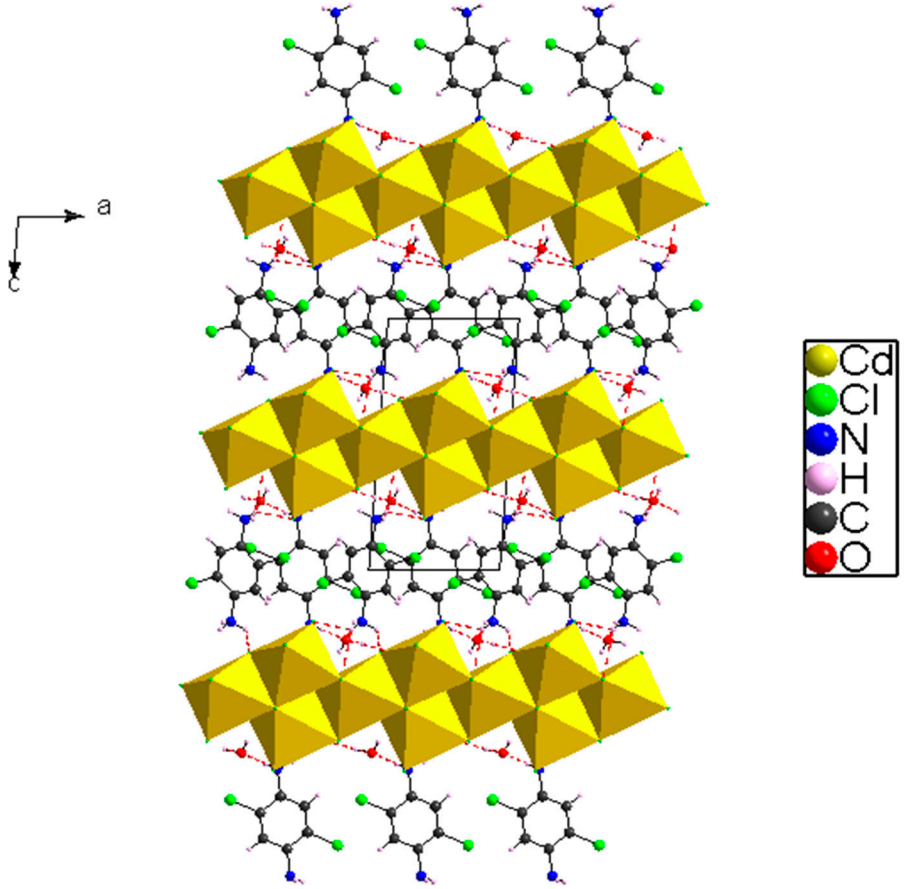

Figure 4. View of $(C_6H_8Cl_2N_2)_2[Cd_3Cl_{10}]\cdot 6H_2O$ along the $\vec{b}$ direction.

The average values of the distortion parameters of the $[CdCl_6]^{2-}$ octahedra were calculated using Equations (1) and (2), respectively:

$$ID(Cd-Cl) = \sum_{i=1}^{n1} \frac{|di - dm|}{n1dm}, \quad (1)$$

$$ID(Cl-Cd-Cl) = \sum_{i=1}^{n2} \frac{|ai - am|}{n2am}, \quad (2)$$

where d is the (Cd-Cl) distance, a is the (Cl-Cd-Cl) angle, m is the average value, n1 = 6 and n2 = 12. The value of the distortion indices were ID(Cd-Cl) = 0.044 and ID(Cl-Cd-Cl) = 0.0026 for $Cd(1)Cl_6$ and ID(Cd-Cl) = 0.063 and ID(Cl-Cd-Cl) = 0.0026 for $Cd(2)Cl_6$. These low values highlight the distorted octahedron geometry of the metal.

On the other hand, the organic part of $(C_6H_8Cl_2N_2)_2[Cd_3Cl_{10}]\cdot 6H_2O$ is made by two crystallographic independent $[C_6H_8Cl_2N_2]^{2+}$ dictations. The cations containing C17, C18 and C19 carbon atoms (molecule A) are located at (0,0,0), while those formed by C15, C16 and C20 (molecule B) carbon atoms are located over the inversion center at (1/2,1/2,0) and are linked to the water molecules via N-H ... O and O-H ... O hydrogen bonds to form ribbons extending along the *c*-axis and located at y = $\frac{1}{2}$ (Figure 6). It is worth mentioning that all organic molecules are parallel to each other and are stacked in an offset manner, but there is nevertheless a degree of π-π overlap between adjacent rings since the distance between two organic cations corresponds to a unit cell, equal to 6.784(4), while the interaction C-Cl ... π could be considered since the shortest distance between the centroid of the ring and chloride atom is 3.504 Å [29,30].

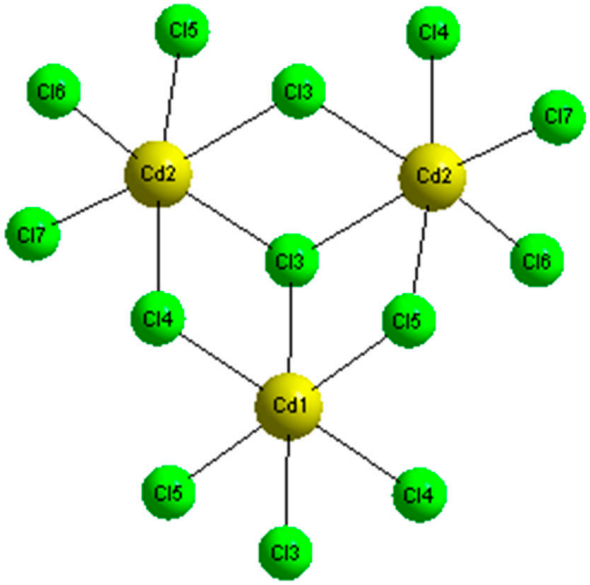

Figure 5. The $[Cd_3Cl_{10}]^{4-}$ trimer coordination.

The main geometrical characteristics of these entities, grouped in Table 3, agree with that found in the literature [31–34].

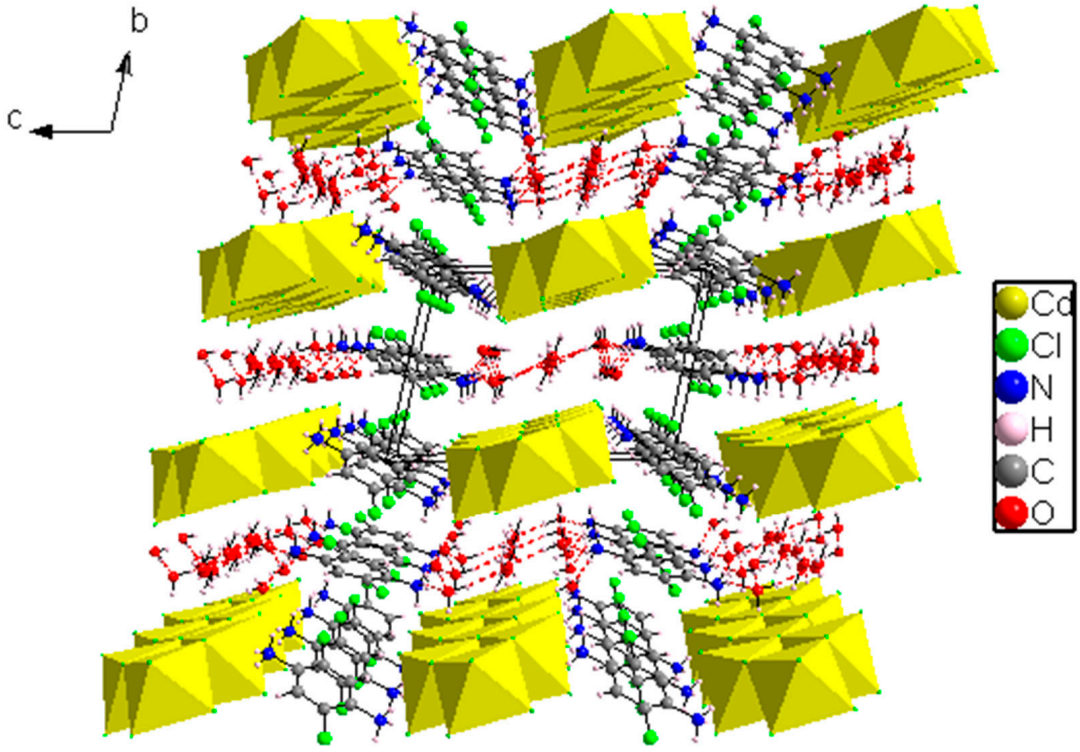

Figure 6. Perspectiveviewof $(C_6H_8Cl_2N_2)_2[Cd_3Cl_{10}]\cdot 6H_2O$.

Table 2. Distances and angles of Cd_3Cl_{10} in $(C_6H_8Cl_2N_2)_2[Cd_3Cl_{10}]\cdot 6H_2O$.

Distances (Å) in $[Cd(1)Cl_6]^{2-}$		**Distances (Å) in $[Cd(2)Cl_6]^{2-}$**	
Cd1—Cl3	2.6998 (16)	Cd2—Cl3^{iii}	2.6480 (17)
Cd1—Cl3^{i}	2.6998 (16)	Cd2—Cl3	2.8180 (16)
Cd1—Cl4^{ii}	2.6125 (17)	Cd2—Cl4	2.6471 (16)
Cd1—Cl4^{iii}	2.6125 (17)	Cd2—Cl5	2.6506 (16)
Cd1—Cl5^{i}	2.5857 (15)	Cd2—Cl6	2.5269 (15)
Cd1—Cl5	2.5857 (15)	Cd2—Cl7	2.5681 (16)
Angles (°) in $[Cd_3Cl_{10}]^{4-}$			
Cl3—Cd1—Cl3^{i}	180.0	Cl4—Cd2—Cl3	91.58 (3)
Cl4^{ii}—Cd1—Cl3	95.52 (3)	Cl4—Cd2—Cl3^{iii}	84.83 (3)
Cl4^{iii}—Cd1—Cl3^{i}	95.52 (3)	Cl5—Cd2—Cl3	82.78 (3)
Cl4^{ii}—Cd1—Cl3^{i}	84.48 (3)	Cl5—Cd2—Cl3^{iii}	89.82 (3)
Cl4^{iii}—Cd1—Cl3	84.48 (3)	Cl5—Cd2—Cl4	172.55 (3)
Cl4^{iii}—Cd1—Cl4^{ii}	180.0	Cl6—Cd2—Cl3	84.46 (3)
Cl5—Cd1—Cl3^{i}	93.63 (3)	Cl6—Cd2—Cl3^{iii}	168.21 (3)
Cl5—Cd1—Cl3	86.37 (3)	Cl6—Cd2—Cl4	90.00 (3)
Cl5^{i}—Cd1—Cl3^{i}	86.37 (3)	Cl6—Cd2—Cl5	94.27 (3)
Cl5^{i}—Cd1—Cl3	93.63 (3)	Cl7—Cd2—Cl3	172.96 (3)
Cl5—Cd1—Cl4^{ii}	89.73 (3)	Cl7—Cd2—Cl3^{iii}	94.57 (3)
Cl5^{i}—Cd1—Cl4^{iii}	89.73 (3)	Cl7—Cd2—Cl4	95.40 (3)
Cl5—Cd1—Cl4^{iii}	90.27 (3)	Cl7—Cd2—Cl5	90.18 (3)
Cl5^{i}—Cd1—Cl4^{ii}	90.27 (3)	Cl7—Cd2—Cl6	96.47 (3)
Cl5^{i}—Cd1—Cl5	180.0	Cd2—Cl3—Cd1^{i}	91.97 (3)
Cd2—Cl4—Cd1^{vi}	96.39 (3)	Cd2^{iii}—Cl3—Cd1^{i}	94.30 (3)
Cd2—Cl5—Cd1^{i}	98.57 (3)		

Symmetrycodes: (i) −x+2, −y, −z+1; (ii) x+1, y, z; (iii) −x+1, −y, −z+1; (vi) x−1, y, z.

Table 3. Geometric feature of $(C_6H_8Cl_2N_2)^{2+}$ in $(C_6H_8Cl_2N_2)_2[Cd_3Cl_{10}]\cdot 6H_2O$.

Distances (Å) in $(C_6H_8Cl_2N_2)^{2+}$			
Cl8—C18	1.727 (4)	Cl9—C20	1.731 (4)
N13—C17	1.477 (5)	N14—C15	1.452 (5)
C17—C18	1.388 (5)	C15—C16	1.393 (5)
C17—C19	1.376 (5)	C15—C20	1.395 (6)
C18—C19	1.388 (5)	C16—C20	1.385 (6)
Angles (°) in $(C_6H_8Cl_2N_2)^{2+}$			
C18—C17—N13	120.7 (3)	C16—C15—N14	120.0 (4)
C19—C17—N13	118.0 (3)	C20—C15—N14	120.6 (3)
C19—C17—C18	121.1 (4)	C20—C15—C16	119.4 (4)
C17—C18—Cl8	120.4 (3)	C20—C16—C15	119.4 (4)
C19—C18—Cl8	120.1 (3)	C15—C20—Cl9	118.8 (3)
C19—C18—C17	119.4 (4)	C16—C20—Cl9	120.0 (3)
C18—C19—C17	119.5 (3)	C16—C20—C15	121.2 (4)

Table 4. H-bond characteristic (Å, °).

D-H ... A	D-H	H ... A	D ... A	D-H ... A
N14—H14*a* ... O11^{vii}	0.88 (3)	1.88 (3)	2.768 (5)	178 (3)
N14—H14*c* ... O12^{viii}	0.88 (3)	1.99 (3)	2.851 (5)	164 (2)
N13—H13b ... O11^{vi}	0.97 (4)	2.01 (4)	2.946 (6)	162 (4)
N14—H14*b* ... Cl6^{ix}	0.99 (2)	2.19 (4)	3.118 (5)	156 (6)
N13—H13a ... Cl5^{i}	0.98 (6)	2.66 (5)	3.200 (5)	115 (3)
N13—H13a ... Cl6^{v}	0.98 (6)	2.35 (5)	3.139 (4)	138 (4)
O11—H11*b* ... O12^{ii}	0.93 (5)	1.80 (5)	2.728 (4)	174 (5)
O12—H12*b* ... O10*A*	0.90 (6)	1.93 (6)	2.817 (15)	174 (6)
O12—H12*b* ... O10*B*^{iii}	0.90 (6)	2.03 (6)	2.878 (14)	157 (6)

Symmetry codes: (i) −x+1, −y+1, −z+1; (ii) x+1, y, z; (iii) −x+1, −y+1, −z+1; (v) x+1, y, z; (vi) −x+1, −y, −z+1, (vii) x, y, z+1; (viii) x−1, y, z+1; (ix) −x, −y+1, −z+2.

3.4. Hirshfeld Surface

(HS) analysis was carried out for decoding and quantifying the intermolecular contributions in the solid material using Crystal Explorer 17.5 [35]. The 2D fingerprint plots are used to highlight a particular atom pain in close contact [36].

The calculation of enrichment ratio for a pair of elements (X, Y) E_{XY} is given in the reference [37], as shown in Table 5.

Figure 7a shows the d_{norm} surface for 2,5-dichloro-p-phenylendiaminium decachlorotricadmate (II) hexahydrate. Herein, the red spots are attributed to the N-H ... O and O-H ... O hydrogen bonds. However, the small flat regions delineated by the blue outline in the surface mapped with curvedness indicate the absence of π ... π stacking interactions in the structure. In addition, there is no evidence of the adjacent red and blue triangles on the shape index surface (Figure 7b,c).

Table 5. Hirshfeld contact surfaces and enrichment ratios for $(C_6H_8Cl_2N_2)_2[Cd_3Cl_{10}]\cdot 6H_2O$.

Atoms	H	Cl	C	Cd	O
Surface%	35.65	39.4	13.45	6.3	1.5
O	2.8	0	0	0	0
Cd	0.04	2.49	0	0	0
C	0.14	0.72	4.9	0	0
Cl	1.38	0.63	0.72	2.49	0
H	1.09	1.38	0.14	0.04	2.8

Figure 8 contains the percentages of the different interactions. The 2D fingerprint plot reveals that H ... Cl/Cl ... H contacts are the most encountered interactions and their relative contribution reaches 38.9%, as shown in Figure 9a, due to the abundance of chloride and hydrogen on the molecular surface (%S_{Cl} = 39.4% and % S_H = 35.65%) with an enrichment ratio E_{HCl} = 1.38. Indeed, the structure cohesion is ensured by three N-H ... Cl hydrogen bonds (Table 4). The H ... H contact represent 13.9% (Figure 9b). The Cd ... Cl/Cl ... Cdis around 12.4% (Figure 9c) with an enrichment ratio E_{CdCl} = 2.49, followed by Cl ... Cl 9.9% (Figure 9d) and C ... C 8.9% (Figure 9e). The Cl ... Cl intermolecular interactions are marked by a low amount of enrichment ratio E_{ClCl} = 0.63 due to the electrostatic repulsion between two charges of the same sign. The C ... C contacts have the most enrichment value, E_{CC} = 4.9, due to the accumulation of aromatic nuclei in the crystalline packing S_C = 13.45%. Other interconnects, such as C ... Cl/Cl ... C 7.7% (Figure 9f), H ... C/C ... H 1.4% (Figure 9h) and Cd ... H/H ... Cd 0.2% (Figure 9i) contributes less to the surface. The C ... Cl, H ... C and Cd ... H interactions are; E_{CCl} = 0.72, E_{HC} = 0.14 and E_{CdH} = 0.04. The low enrichment ratio value reveals that pairs tend to avoid contact with each other. Finally, the percentage of H ... O/H ... O intermolecular interactions is around 3% (Figure 9g) and they are over-represented (E_{HO} = 2.8). Indeed, there are three N-H ... O and three O-H ... O hydrogen bonds in the structure (Table 4).

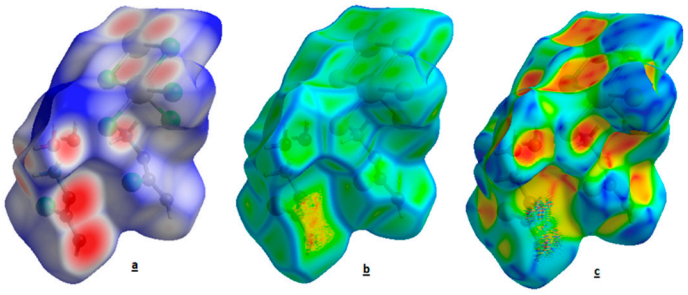

Figure 7. The HS mapped with d_{norm} (**a**). Shape index (**b**) and curvedness (**c**) for the title compound.

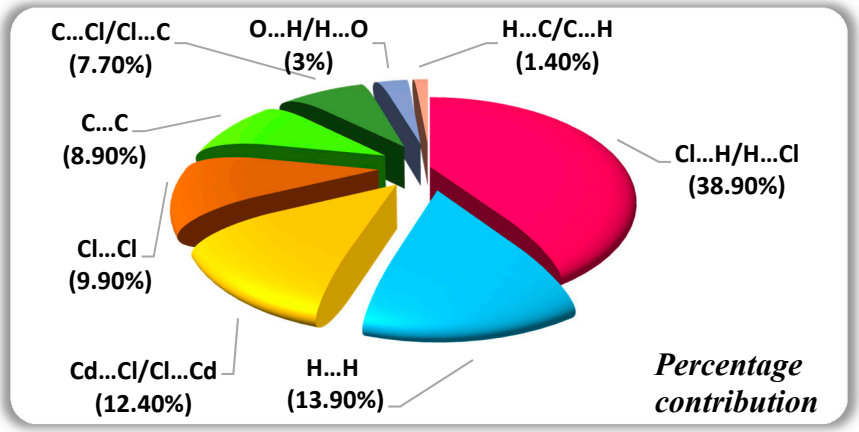

Figure 8. Contacts in $(C_6H_8Cl_2N_2)_2[Cd_3Cl_{10}]\cdot 6H_2O$ crystals.

3.5. Infrared Spectral Studies

The FT-IR was used to verify the functional groups in the synthesized material and their vibrational behavior. Figure 10 display the FT-IR spectrum of $(C_6H_8Cl_2N_2)_2[Cd_3Cl_{10}]\cdot 6H_2O$. Since all bands originating from the vibration of the anions are observed below 400 cm^{-1}, the vibrational spectrum is only due to the cation [38].

The bands at high-frequency domain can be attributed to the N-H, O-H and C-H stretching vibrations. The assignment and the deduction of these bands are based on similar reported results [39,40].

Indeed, the bands observed at 3572 cm^{-1}, 3528 cm^{-1}, and 3496 cm^{-1} are attributed to $\upsilon_{(O\text{-}H)}$ of water molecules confirmed by DFT computations with the frequency at 3498 cm^{-1} and 3420 cm^{-1}. However, the two bands at 3347 and 3401 cm^{-1} are assigned to the stretching vibrations of the N-H group. The DFT calculation predicted these modes in the range 3159 and 3134 cm^{-1}. As matter of fact, hydrogen bonding interactions influence the frequency as well as the intensity and the width of these vibrations. As for the C-H stretching bands, they are assigned generally between 3000 and 2800 cm^{-1} and are visible by DFT computation at 2970 and 3185 cm^{-1}. Moreover, the band between 1590 and 1480 cm^{-1} corresponds to $\delta_{(N\text{-}H)}$ and $\delta_{(O\text{-}H)}$ deformation vibrations. This vibration is well observed by DFT calculations by a large band at 1485 cm^{-1}.

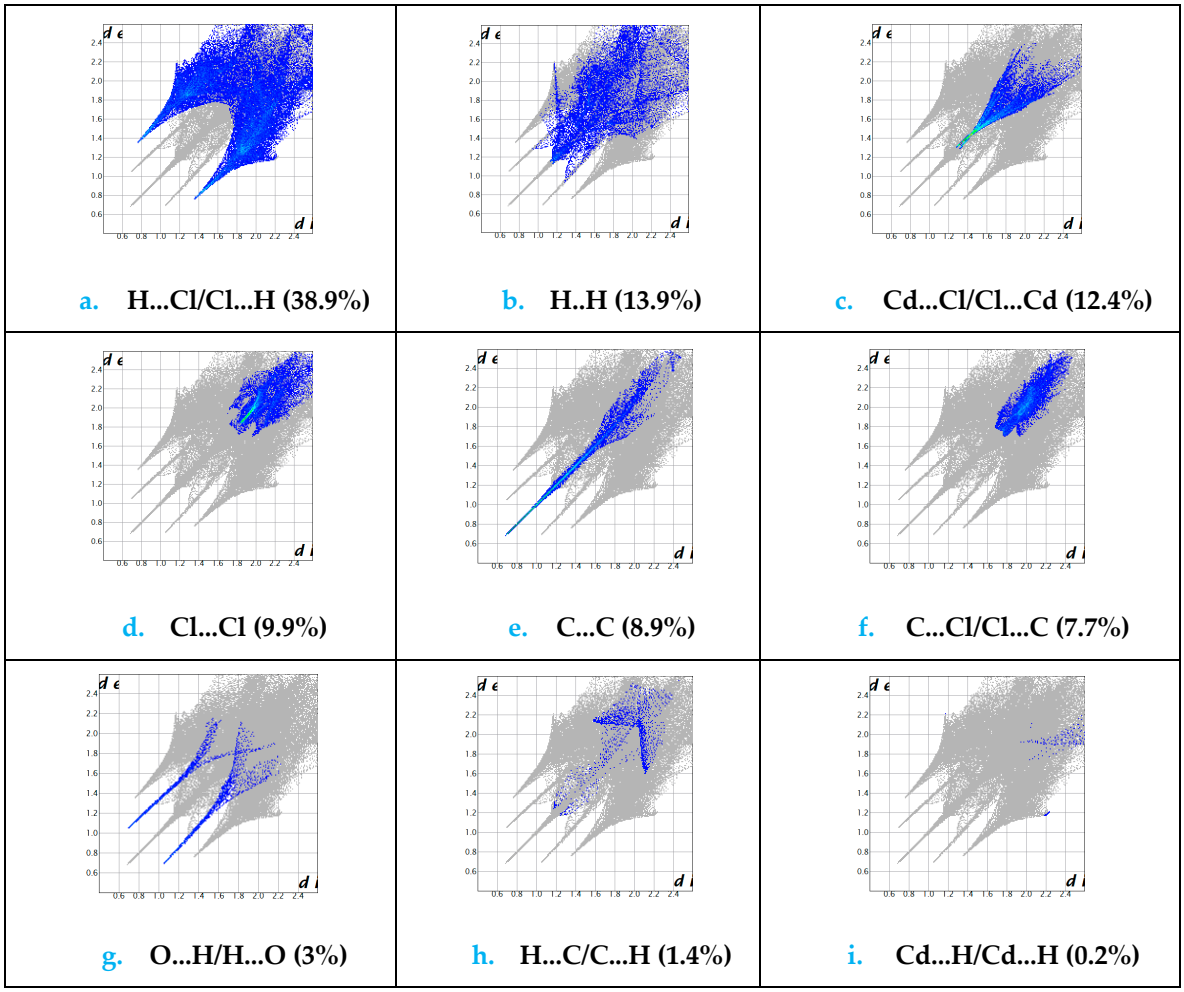

Figure 9. Fingerprint plots showing contribution from different contact. (**a**) H . . . Cl/Cl . . . H, (**b**) H . . . H, (**c**) Cd . . . Cl/Cl . . . Cd, (**d**) Cl . . . Cl, (**e**) C . . . C, (**f**) C . . . Cl/Cl . . . C, (**g**) O . . . H/H . . . O, (**h**) H . . . C/C . . . H, (**i**) Cd . . . H/H . . . Cd.

Furthermore, the vibration band located 1406 cm^{-1} is assigned to the $\upsilon_{(C=C)}$ aromatic ring stretching vibrations, this vibration is well-observed by the DFT calculation and was found at 1421 cm^{-1}. The vibration at 1103 cm^{-1} corresponds to aromatic C-H in plan bending mode and it is confirmed by DFT calculations at 1080 cm^{-1}. Moreover, the band at 817 cm^{-1} corresponds to the out of plan bending of the benzene ring, which is consistent with the proposed tetra-substituted benzene ring. The vibration bands between 1292 cm^{-1} and 1172 cm^{-1} are attributed to valence vibrations of $\upsilon_{(C-N)}$, DFT calculations predicted this mode at 1350 cm^{-1} and at 1250 cm^{-1}. Additionally, the C-Cl stretching frequencies are seen at 875 cm^{-1}. However, the $\rho_{(C-H)}$ and $\omega_{(N-H)}$ vibrations bands appear at 650 cm^{-1} and 500 cm^{-1} as weak bands, and this was calculated to be found in the region 1000 to 500 cm^{-1} and they are weakly visible.

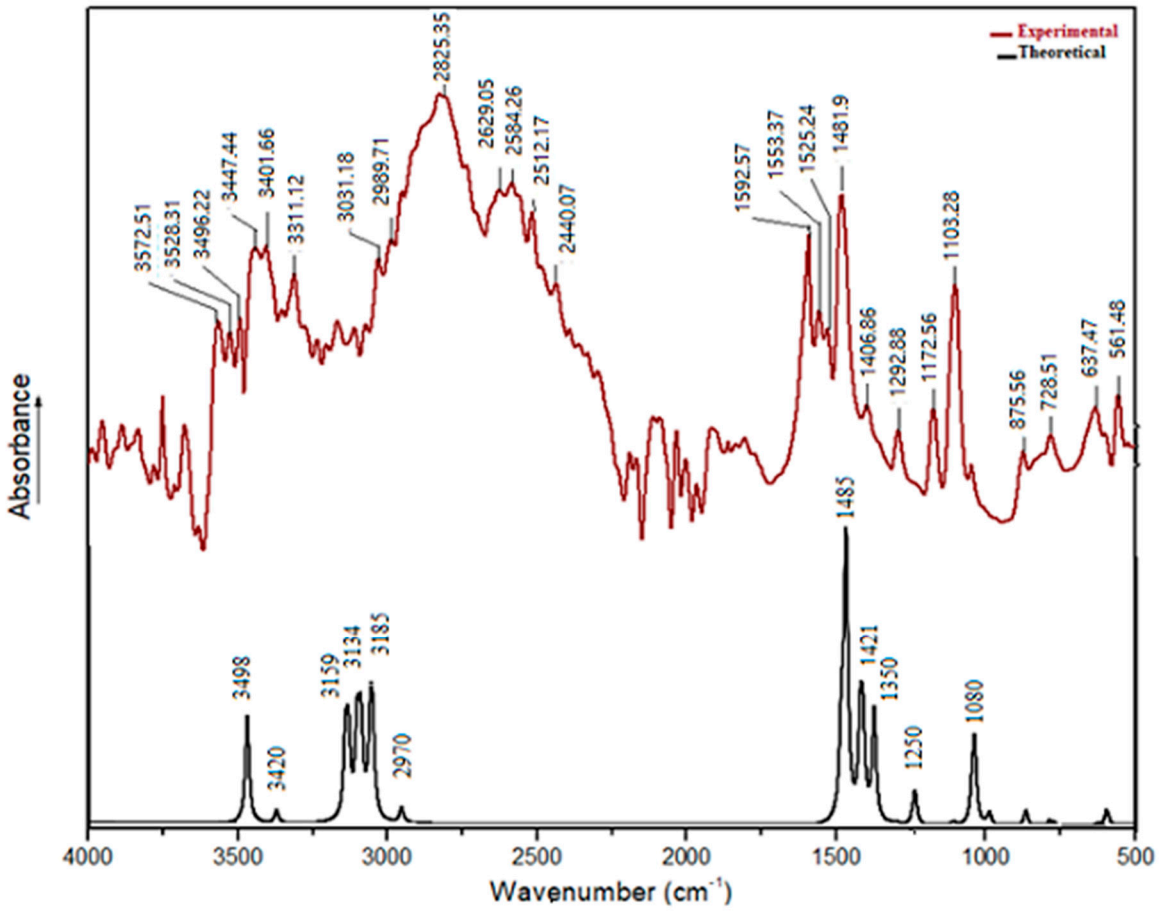

Figure 10. Infrared absorption spectrum of $(C_6H_8Cl_2N_2)_2[Cd_3Cl_{10}]\cdot 6H_2O$.

The DFT-IR spectrum and the experimental spectrum, given in Figure 10, are very similar. In Figure 11 a nice straight-line correlation was observed. It is worth considering that when comparing both experimental and theoretical results, the theoretically predicted parameters were calculated in a simulated water phase, and this latter is so far from the experimental environment. Subsequently, small deviations should not be surprising. Even so, the results demonstrate a good agreement, which is well-confirmed by the correlation (R^2 = 0.987) that is mostly achieved in the fingerprint region.

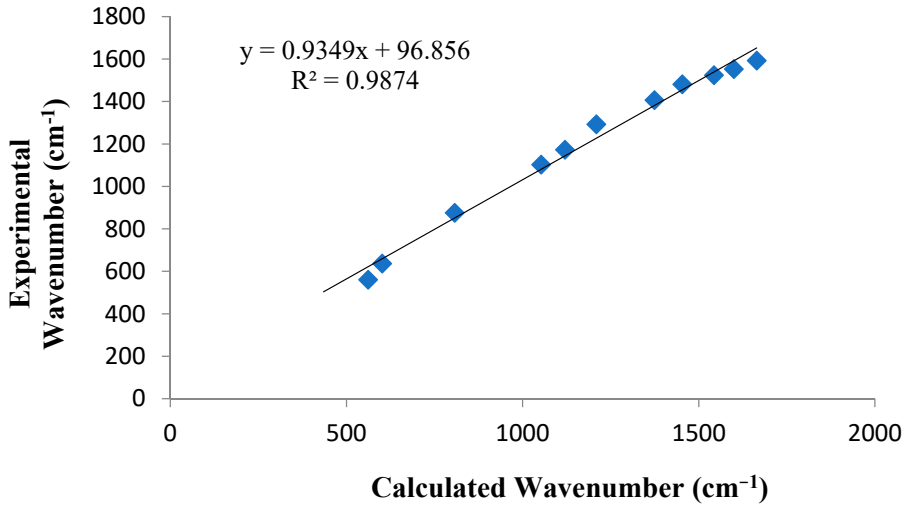

Figure 11. Calculated vs. experimental wavenumbers of $(C_6H_8Cl_2N_2)_2[Cd_3Cl_{10}]\cdot 6H_2O$.

3.6. Quantum Mechanical Study of $(C_6H_8Cl_2N_2)_2[Cd_3Cl_{10}]\cdot 6H_2O$

The HOMO and LUMO molecular orbitals were determined (Figure 12). As it can be seen, the HOMO-LUMO energy difference is very small, around 0.2 eV, which seems to indicate a weak stability. The HOMO is localizedon the inorganic part of the system, while the LUMO islocated on the organic and the inorganic parts, which will lead to electronic transfers from one to the other. The (DOS)energy is represented in Figure 13.

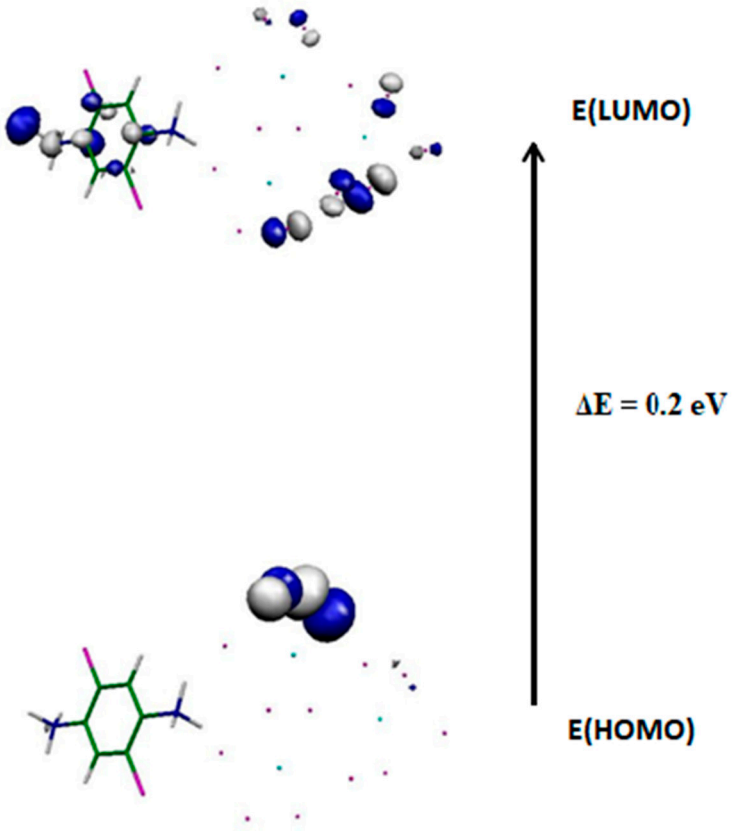

Figure 12. Frontier molecular orbitals in $(C_6H_8Cl_2N_2)_2[Cd_3Cl_{10}]\cdot 6H_2O$.

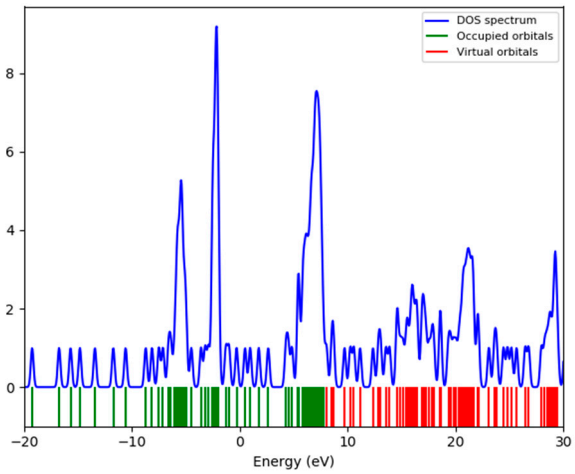

Figure 13. The DOS spectrum of $(C_6H_8Cl_2N_2)_2[Cd_3Cl_{10}]\cdot 6H_2O$.

3.7. Molecular Electrosatatic Ootential (MEP) Analysis

The MEP map is used to identify the active sites of a given molecule. For this reason, MEP mapped surface of this compound is shown in Figure 14. As it can be seen, the electrostatic potential maps are colour-coded and are subdivided into many regions. The

blue and red colours indicate the positive and negative potentials, respectively. The inorganic part is negative, while the organic entity is positive. These results agree with Mulliken charges (Table 6).

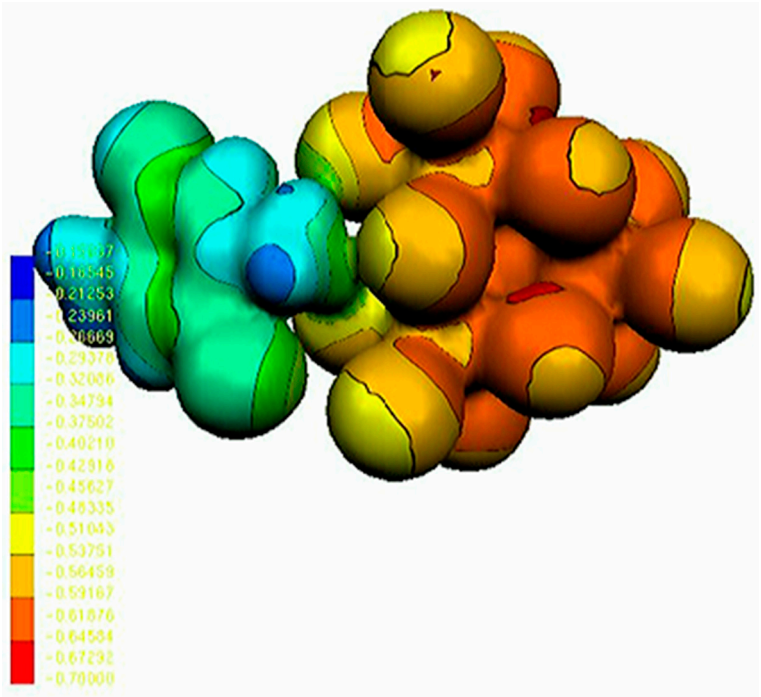

Figure 14. MEP surface of $(C_6H_8Cl_2N_2)_2[Cd_3Cl_{10}]\cdot 6H_2O$.

3.8. Mulliken Population Analysis of $(C_6H_8Cl_2N_2)_2[Cd_3Cl_{10}]\cdot 6H_2O$

The Mulliken charge distribution of all atoms is shown in Table 6. The underlined atoms are those that are interacting in the Cd_3Cl_{13} + Ligand 2 system. The transfer occurs to the para atoms of those where the interaction takes place (carbon 2 and other nitrogen). The atoms of the organic molecule are numbered as depicted in Figure 15.

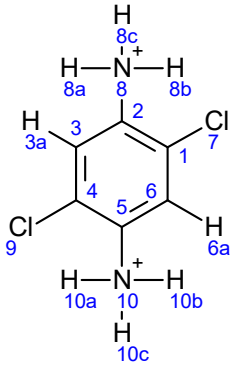

Figure 15. The atoms numbering of the organic molecule.

For the Cd_3Cl_{13}anion, the cadmium ions have positive charges, while all chlorine atoms have negative charges. For the organic cations, Cl7 has a negative charge of −0.075, while Cl9 has a positive charge of 0.262. The nitrogen atoms N8 have a positive charge of 1.487, while the N10 has a negative charge of −1.070. The carbon atoms C1, C5 and C6 have positive charges, while C2, C3 and C4 have negative charges. It is worth noting that hydrogen atoms in the range 0.206–0.523 carry a positive charge.

Table 6. Mulliken charge distribution in $(C_6H_8Cl_2N_2)_2[Cd_3Cl_{10}]\cdot 6H_2O$.

Atom	Mulliken Charge
C1	1.331123
C2	−4.737247
C3	−1.070936
H(C3)	0.206980
C4	−1.443429
C5	0.547071
C6	1.649255
H(C6)	0.271790
Cl7	−0.075264
Cl9	0.262067
N8	1.487065
H(N8)	0.380289 0.392109 0.403416
N10	−1.070241
H(N10)	0.523128 0.497461 0.479144
Cd	1.202720 1.335296 1.175898
Cl	−0.680423 −0.919000 −0.747317 −0.452354 −0.606892 −0.576617 −0.534910 −0.845237 −0.556969 −0.728453 −0.787878 −0.596435 −0.715207

3.9. Thermal Analysis

Thermal analysis is one of the most useful methods of analysis in collecting both physical and chemical information. For this reason, we chose (TG/DTA), the most used technique of thermal analysis in providing information about the bonding of components within the sample. The TGA and DTA measurements, in the range 200–1200 K, are depicted in Figure 16.

The first peak in the DTA curve occurred at 380 K with ΔH = 994.99 $J.g^{-1}$, corresponding to the complete dehydration of the compound. It is accompanied by a weight loss observed in the TGA curve equal to 7.78% (calculated weight loss: 7.79%). While the three endothermic peaks observed in the DTA curve at 452, 535, and 600 K correspond to the decomposition of the organic matrix with a total experimental weight loss equal to 30.94% and calculated weight loss: 30.92%. Then, the DTA curve presents a sharp endothermic peak, centered at 919 K, corresponding to the degradation of the inorganic group (exp.loss: 59.60%/thero. loss: 59.74%). At the end of the experience, the obtained solid is a black residuethat represents1.68% of the initial mass.

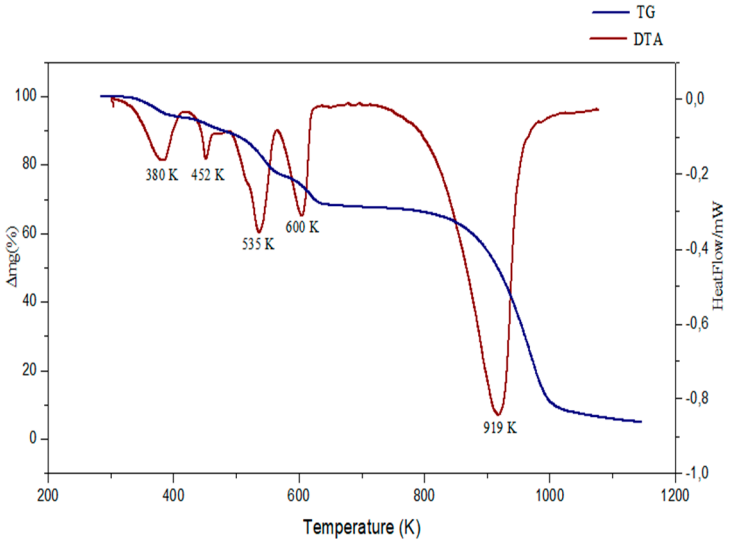

Figure 16. TGA/DTA curves of $(C_6H_8Cl_2N_2)_2[Cd_3Cl_{10}]\cdot 6H_2O$.

4. Conclusions

A new hybrid material of cadmium with 2,5-dichloro-p-phenylenediamine has been synthesized in an aqueous solution at room temperature. XRD analysis shows that 2,5-dichloro-p-phenylendiaminium decachlorotricadmate(II) hexahydrate crystallizes in the triclinic crystal system $P\bar{1}$, the different entities are held together by columbic attraction and multiple hydrogen bonds to form a three-dimensional network. The Hirshfeld surface analysis and the 2D fingerprint plots were performed and highlight that Van der Waal forces exert an important role on the stabilization in the crystal structure. Scanning electronic microscopy (SEM) was carried out and the EDX spectrum of the title compound revealed the presence of all non-hydrogen atoms. The powder XRD is in agreementwith single-crystal. Structural and spectroscopic proprieties were investigated by FT-IR spectroscopy as well as by DFT calculation. The MEP map defines the nucleophile and the electrophile sites. The HOMO-LUMO energy gap proposes a good electric conductivity. Finally, the thermal stability is proved by TGA/DTA thermal analysis.

Author Contributions: Formal analysis, W.F.; Funding acquisition, M.G.A.; Investigation, C.B.N.; Resources, A.A.A.; Software, A.H.A. and F.L.; Supervision, M.H.M.; Writing—original draft, S.H. All authors have read and agreed to the published version of the manuscript.

Funding: This research received no external funding.

Acknowledgments: Authors thank Taif University Researchers Supporting Project Number (TURSP-2020/272) Taif University, Taif, Saudi Arabia.

Conflicts of Interest: The funders had no role in the design of the study; in the collection, analyses, or interpretation of data; in the writing of the manuscript, or in the decision to publish the results.

References

1. Zhou, C.; Lin, H.; Neu, J.; Zhou, Y.; Chaaban, M.; Lee, S.; Worku, M.; Chen, B.; Clark, R.J.; Cheng, W. Green Emitting Single-Crystalline Bulk Assembly of Metal Halide Clusters with Near-Unity Photoluminescence Quantum Efficiency. *ACS Energy Lett.* **2019**, *4*, 1579–1583. [CrossRef]
2. Aguirre-Díaz, L.M.; Reinares-Fisac, D.; Iglesias, M.; Gutiérrez-Puebla, E.; Gándara, F.; Snejko, N.; Monge, M.Á. Group 13th metal-organic frameworks and their role in heterogeneous catalysis. *Coord. Chem. Rev.* **2017**, *335*, 1–27. [CrossRef]
3. Li, J.R.; Tao, Y.; Yu, Q.; Bu, X.-H.; Sakamoto, H.; Kitagawa, S. Selective gas adsorption and unique structural topology of a highly stable guest-free zeolite-type MOF material with N-rich chiral open channels. *J. Chem. Eur.* **2008**, *14*, 2771–2776. [CrossRef] [PubMed]
4. Li, X.; Wu, B.L.; Niu, C.Y.; Niu, Y.Y.; Zhang, H.Y. Syntheses of Metal-2-(Pyridin-4-yl)-1H-imidazole-4,5-dicarboxylate networks with topological diversity: Gas adsorption, thermal stability and fluorescent emission properties. *J. Cryst. Growth* **2009**, *9*, 3423–3431. [CrossRef]

5. Brzostek, K.S.; Terlecki, M.; Sokołowski, K.; Lewinski, J. Chemical fixation and conversion of CO_2 into cyclic and cage-type metal carbonates. *Coord. Chem. Rev.* **2017**, *334*, 199–231. [CrossRef]
6. Hu, Z.; Deibert, B.J.; Li, J. Luminescent metal–organic frameworks for chemical sensing and explosive detection. *Chem. Soc. Rev.* **2014**, *43*, 5815–5840. [CrossRef] [PubMed]
7. Patra, R.; Titia, H.M.; Goldberg, I. Coordination polymers of flexible polycarboxylic acids with metal ions. V. polymeric frameworks of 5-(3,5-dicarboxybenzyloxy)-3-pyridine carboxylic acid with Cd(ii), Cu(ii), Co(ii), Mn(ii) and Ni(ii) ions; synthesis, structure, and magnetic properties. *CrystEngComm* **2013**, *15*, 2863–2872. [CrossRef]
8. Allen, F.H.; Kennard, O. Cambridge crystallographic data file. *J. Autom. Chem.* **1993**, *8*, 31–37.
9. Brammer, L.; Swearingen, J.K.; Bruton, E.A.; Sherwood, P. Hydrogen bonding and perhalometallate ions: A supramolecular synthetic strategy for new inorganic materials. *Proc. Natl. Acad. Sci. USA* **2002**, *99*, 4956–4961. [CrossRef]
10. Moulton, B.; Zaworotko, M.J. From molecules to crystal engineering: Supramolecular isomerism and polymorphism in network solids. *Chem. Rev.* **2001**, *6*, 1629–1658. [CrossRef]
11. Badawi, H.M.; Förner, W.; Ali, S.A. A comparative study of the infrared and Raman spectra of aniline and o-, m-, p-phenylenediamine isomers. *Spectrochim. Acta Part A* **2013**, *112*, 388–396. [CrossRef]
12. Cao, Y.; Smith, P.; Heeger, A.J. Counter-ion induced processibility of conducting polyaniline and of conducting polyblends of polyaniline in bulk polymers. *Synth. Met.* **1992**, *48*, 91–97. [CrossRef]
13. Guo, T.; Wang, L.; Evans, D.G.; Yang, W. Synthesis and Photocatalytic Properties of a Polyaniline-intercalated layered protonic titanate nanocomposite with ap− n heterojunction structure. *J. Phys. Chem. C* **2010**, *114*, 4765–4772. [CrossRef]
14. Li, T.; Yuan, C.; Zhao, Y.; Chen, Q.; Wei, M.; Wang, Y. Synthesis, characterization, and properties of aniline-p-phenylenediamine copolymers. *High Perform. Polym.* **2013**, *25*, 348–353. [CrossRef]
15. Sharma, R.P.; Singh, A.; Venugopalan, P.; Yanan, G.; Yu, J.; Angeli, C.; Ferretti, V. Caging Anions through Crystal Engineering to Avoid Polymerization: Structural, Conformational and Theoretical Investigations of New Halocadmate $[Cd_2X_7]^{3-}$ Anions (X = Cl/Br). *Eur. J. Inorg. Chem.* **2012**, *8*, 1195–1203. [CrossRef]
16. Luo, J.; Hong, M.; Wang, R.; Cao, R.; Shi, Q.; Weng, J. Self-Assembly of Five Cadmium (II) Coordination Polymers from 4,4′-Diaminodiphenylmethane. *Eur. J. Inorg. Chem.* **2003**, *9*, 1778–1784. [CrossRef]
17. Bonnamartini, C.A.; Ferrari, A.M.; Pellacani, G.C. Organic-inorganic composite materials: Structural archetypes of linear polymeric chlorocadmates (II). *Inorg. Chim. Acta* **1998**, *272*, 252–260.
18. Mercier, N.; Louvain, N.; Wenhua, B. Structural diversity and retro-crystal engineering analysis of iodometalate hybrids. *CrystEngComm* **2009**, *11*, 720–734. [CrossRef]
19. CrystalClear. In *Data Collection and Processing Software*; Rigaku Corporation: Tokyo Japan, 1998–2014; pp. 196–8666.
20. Bourhis, L.J.; Dolomanov, O.V.; Gildea, R.J.; Howard, J.A.K.; Puschmann, H. The anatomy of a comprehensive constrained, restrained refinement program for the modern computing environment-*Olex2* dissected. *Acta Cryst. Sect. A.* **2015**, *71*, 59–75. [CrossRef] [PubMed]
21. Crystal Structure 4.1. In *Crystal Structure Analysis Package*; Rigaku Corporation: Tokyo, Japan, 2000–2014; pp. 196–8666.
22. Brandenburg, K. *Diamond Version 2.0*; Impact GbR: Bonn, Germany, 1998.
23. Macrae, C.F.; Edgington, P.R.; McCabe, P.; Pidcock, E.; Shields, G.P.; Taylor, R.; Towler, M.; Van de Streek, J. Mercury: Visualization and analysis of crystal structures. *J. Appl. Crystallogr.* **2006**, *39*, 453–457. [CrossRef]
24. Lassoued, M.S.; Abdelbaky, M.S.; Ammar, S.; Salah, A.B.; Gadri, A.; García-Granda, S. Preparation, molecular structure, vibrational and photoluminescence study of a novel compound based chlorocadmate (II) material. *J. Mol. Struct.* **2018**, *1165*, 42–50. [CrossRef]
25. Chaabane, I.; Hlel, F.; Guidara, K. Synthesis, Infra-red, Raman, NMR and structural characterization by X-ray Diffraction of $[C_{12}H_{17}N_2]_2$ $CdCl_4$ and $[C_6H_{10}N_2]_2Cd_3Cl_{10}$ compounds. *PMC Phys. B* **2008**, *1*, 1–19. [CrossRef]
26. Dhieb, A.C.; Dridi, I.; Mathlouthi, M.; Rzaigui, M.; Smirani, W. Structural Physico Chemical Studies and Biological Analyses of a Cadmium Cluster Complex. *J. Clust. Sci.* **2018**, *29*, 1123–1131. [CrossRef]
27. Gagor, A.; Waśkowska, A.; Czapla, Z.; Dacko, S. Structural phase transitions in tetra (isopropylammonium) decachlorotricadmate (II), $[(CH_3)_2CHNH_3]_4Cd_3Cl_{10}$, crystal with a two-dimensional cadmium (II) halide network. *Acta Crystallogr. Sect. B* **2011**, *67*, 122–129. [CrossRef] [PubMed]
28. El Glaoui, M.; Kefi, R.; Lefebvre, F.; Jeanneau, E.; Ben Nasr, C. Crystal structure and spectroscopic studies of an inorganic-organic hybrid compound $(C_6H_{10}N_2)_2(Cd_3Cl_{10})\cdot 4H_2O$. *Can. J. Anal. Sci. Spectros.* **2008**, *53*, 241–248.
29. Mitra, D.; Namrata, B.; Daliah, M.; Sekar, K. C-halogen ... pi interactions in nucleic acids: A database study. *J. Chem. Soc.* **2020**, *132*, 1–6.
30. Tan, S.L.; Lee, S.M.; Lo, K.M.; Otero-de-la-Roza, A.; Tiekink, E.R. Experimental and computational evidence for a stabilising C–Cl(lone-pair)π(chelate-ring) interaction. *CrystEngComm* **2021**, *23*, 119–130. [CrossRef]
31. Ruhland, V.; Christopher, J. The Molecular Basis of Modern Marker Chemistry. Ph.D. Thesis, Cardiff University, Cardiff, UK, 2011.
32. Yang, Q.C.; Tang, Y.Q.; Yang, W.J.; Chen, H.Y. N-(3-Nitrobenzylidene)-p-phenylenediamine. *Acta Crystallogr. Sect. C* **1998**, *54*, 1532–1534. [CrossRef]
33. Glomm, B.H.; Rutledge, G.C.; Küuchenmeister, F.; Neuenschwander, P.; Sute, U.W. Spinning and characterization of fibers from poly (2,6-dichloro-p-phenyleneterephthalamide): A study of constitutional isomerism and solid-state arrangements by comparison between simulation and experiment. *Macromol. Chem. Phys.* **1994**, *195*, 475–510. [CrossRef]

34. Seth, S.K.; Sarkar, D.; Roy, A.; Kar, T. Insight into supramolecular self-assembly directed by weak interactions in acetophenone derivatives: Crystal structures and Hirshfeld surface analyses. *CrystEngComm* **2011**, *13*, 6728–6741. [CrossRef]
35. Spackman, M.A.; Dylan, J. Hirshfeld surface analysis. *CrystEngComm* **2009**, *11*, 19–32. [CrossRef]
36. McKinnon, J.J.; Spackman, M.A.; Anthony, S.M. Novel tools for visualizing and exploring intermolecular interactions in molecular crystals. *Acta Crystallogr. Sect. B.* **2004**, *60*, 627–668. [CrossRef] [PubMed]
37. Jelsch, C.; Ejsmont, K.; Huder, L. The enrichment ratio of atomic contacts in crystals, an indicator derived from the Hirshfeld surface analysis. *IUCrJ* **2014**, *1*, 119–128. [CrossRef] [PubMed]
38. Hajji, M.; Kouraichi, C.; Guerfel, T. Modelling, structural, thermal, optical and vibrational studies of a new organic–inorganic hybrid material $(C_5H_{16}N_2)Cd_{1.5}Cl_5$. *Bull. Mater. Sci.* **2017**, *40*, 55–66. [CrossRef]
39. Kolcu, F.; Kaya, İ. A study of the chemical and the enzyme-catalyzed oxidative polymerization of aromatic diamine bearing chlor substituents, pursuant to structural, thermal and photophysical properties. *Eur. Polym. J.* **2020**, *133*, 109767. [CrossRef]
40. Wang, G.E.; Wang, M.S.; Jiang, X.M.; Liu, Z.F.; Lin, R.G.; Cai, L.Z.; Guo, G.C.; Huang, J.S. Crystal structures and optical properties of 1-D iodoplumbates templated by in situ synthesized p-phenylenediamine derivatives. *Inorg. Chem. Commun.* **2011**, *14*, 1957–1961. [CrossRef]